# Analysis of the radial transport of tracers in a turbulence simulation

G. Sánchez Burillo,[1] B. Ph. van Milligen,[1] and A. Thyagaraja[2]
[1]*Asociación EURATOM-CIEMAT para Fusión, Avda. Complutense 22, 28040 Madrid, Spain*
[2]*EURATOM-UKAEA Fusion Association, Culham Science Centre, Abingdon OX14 3DB, United Kingdom*

(Received 20 November 2008; accepted 23 March 2009; published online 30 April 2009)

It has been suggested that radial transport in turbulent plasmas may be nonlocal and non-Markovian. In this paper the transport of test particles in the global, electromagnetic, three-dimensional code CUTIE [A. Thyagaraja *et al.*, Phys. Plasmas **12**, 090907 (2005)] is characterized. This code includes a nonlinear feedback mechanism between the meso- and macroscales that are expected to lead to some degree of self-organization that should be reflected in the trajectories of the tracer particles. Several techniques are used to analyze these trajectories, and indeed long-range spatial and temporal correlations are detected, indicating that effective global radial transport in CUTIE does not satisfy the traditional paradigm of diffusive transport. Part of this result can be explained from the existence of propagating ballistic events, and another part from a dependence of local transport properties on the safety factor: local transport is found to depend sensitively on the position relative to specific rational surfaces. © *2009 American Institute of Physics*. [DOI: 10.1063/1.3118589]

## I. INTRODUCTION

The radial transport of particles in fusion-grade plasmas is still not fully understood. The test particle approach provides a way to probe transport systematically and compare results with theoretical expectations. Additionally, the net transport properties obtained in this way may provide input for the future development of simplified effective transport models.

In this work, we follow and expand the work of other authors[1–4] by launching tracer particles in a simulation of plasma turbulence. The resulting tracer trajectories are then analyzed by means of several techniques. These techniques are based on the ideas provided by the well-established field of continuous time random walks (CTRWs),[5,6] which includes a wide range of transport models going beyond the limits of Markovian and local transport models.[7–11]

In the one-dimensional CTRW model, particle motion consists of a series of alternating steps (or jumps) and rests (or trappings): a particle remains at its current position for some time and then performs a jump. Obviously, this is an approximation of actual particle motion (which is continuous). If the system consists of identical particles such that a probabilistic description is feasible, motion is governed by a joint probability distribution function (pdf) $\xi$ giving the probability of occurrence of jumps and trappings.[9] Assuming the jumps and trappings are independent, $\xi$ is separable and, assuming invariance under space and time translations, it can be written as $\xi=p(\Delta x)\cdot\psi(\Delta t)$: here, $p$ is the step size pdf or the probability of performing a step $\Delta x$ and $\psi$ is the waiting time pdf or the probability of waiting for a time lapse $\Delta t$.

CTRW models provide a generalization of standard (diffusive) models and can be written in the limit of many particles as a generalized master equation (GME).[12,13] For many CTRWs (and corresponding GMEs), a corresponding effective global transport equation can be derived in the so-called fluid limit (the limit of large temporal and spatial scales), i.e., a fractional differential equation (FDE).[14–21] The existence of these relations between various levels of description of transport (CTRW→GME→FDE) then provides a means of studying transport at a very basic level and verifying whether there is any truth to the claim that transport in fusion plasmas is essentially non-Markovian and nonlocal. All one has to do is inject tracer particles and observe their distribution in space and time; the result is directly related to distributions $p$ and $\psi$ mentioned earlier. In principle, this can be done both in numerical simulations and in actual experiments, although the latter may present some formidable practical difficulties. This type of analysis is complicated by the existence of nonhomogeneities (a spatial dependence of $\xi$) in realistic simulations and experiments, which has to be treated carefully.

Here, we study the transport of tracers in the turbulence code CUTIE, which differs from the codes studied in the cited references in that a number of instabilities are modeled simultaneously, and in that the simulation is a full-tokamak simulation, thus providing enhanced realism. As we will show in the following, transport in the CUTIE run that we studied is characterized by radial zones with different characteristics. However, instead of considering these zones separately, we will attempt to find an effective global description of the tracer motion in line with the ideas outlined above regarding the search for an effective simplified transport model.

The CUTIE code[22–24] is an electromagnetic, global two-fluid model for plasma turbulence in tokamaks. The equations used to evolve $T_{e,i}$, $n_e \simeq n_i$, the ion parallel velocity $v$, the electrostatic potential $\Phi$, the parallel vector potential $\Psi$, and the potential vorticity $\Theta$ are described in detail in Refs. 25–27. CUTIE models tokamaks on the "mesoscale." The meso-time-scale is the time scale between the Alfvén time $[t_A=qR/V_A$ with $V_A=B_T/(\mu_0 m_i n_e)^{1/2}]$ and the resistive time $[t_{\mathrm{res}}=a^2/(\varepsilon_0\eta_{\mathrm{nc}})$, where $\eta_{\mathrm{nc}}$ is the neoclassical resistivity], and in space, the mesolength scales $L_{\mathrm{meso}}$ lie in the interval $r_s<L_{\mathrm{meso}}<a$ [where $r_s=C_s/\Omega_i$, $C_i^2=k(T_e+T_i)/m_i$, $\Omega_i=eB_T/m_i$, $m_i$ is the mass of the main ion species, and $e$ is the

 © 2009 American Institute of Physics

Downloaded 11 Aug 2011 to 194.81.223.66. Redistribution subject to AIP license or copyright; see http://pop.aip.org/about/rights_and_permissions

elementary charge]. The model includes the physics of shear Alfvén, drift tearing, and ballooning modes.[27] When subject to electron cyclotron resonance heating power (i.e., an external source), the system gives rise to turbulence with regions of mesoscale variations in the profiles called "corrugations," which interact nonlinearly with the turbulence (as has also been observed in gyrokinetic simulations[28]).

This nonlinear feedback mechanism between turbulence and profiles (i.e., between meso- and macroscales) suggests the existence of self-organization that should be reflected by the tracer trajectories, which should display a degree of self-similarity at least in a certain parameter range. In other words, one expects that the corresponding distribution functions should have a power law decay.

We have launched tracers in CUTIE and calculated their trajectories. At the end of the simulation most tracers stay in the range $0.3 < r/a < 0.8$ because of the presence of internal transport barriers. Thus, the analysis is restricted to this range. Radial motion has been characterized using different analysis techniques to look for long-range correlations in time and space and to measure the power-law decay indices of the distribution functions. These techniques can be divided into two groups. The first involves the analysis of the various particle distribution functions, while the second studies Lagrangian velocity distributions.

We find that transport is globally nonlocal and non-Markovian. In addition, an initially unexpected but interesting relationship is found between some transport magnitudes and the $q$-profile. Large differences are detected in an effective diffusion coefficient on either side of the location of some low-order rational surfaces.

This paper is organized as follows. In Sec. II, we discuss the setup of the study we performed and explain some of the analysis methods we have used. In Sec. III we present the analysis results. Finally, in Sec. IV we will provide a discussion and some conclusions.

## II. SETUP AND METHODS

This section discusses the setup and the analysis methods. First, we discuss the plasma state that was studied. Then, we introduce the tracer algorithm and its implementation in CUTIE. Finally, we explain the various tracer analysis techniques, divided into two groups: the analysis of (a) distribution functions and (b) velocity correlations.

### A. Plasma state studied

Using CUTIE, we ran a simulation corresponding to the device COMPASS[29–31] ($R_0$=56 cm, $a$=24 cm, aspect ratio ≈0.23, $B_0$=2.1 T on axis, plasma current $I_p$=240 kA) with electron cyclotron resonant heating ($P_{\mathrm{ECRH}}$=340 kW). The total simulation time is $\tau_{\mathrm{tot}}$=20 ms. Figure 1(a) shows the electron temperature and density profiles.

Fluctuations are artificially set to zero at $r/a$=1, while the effective plasma edge is taken to be at $r/a$=0.95. In between, a consistent particle/energy sink is included by way of a simplified scrapeoff layer model. Here the equilibrium flux surfaces are concentric circular cylinders. The conditions of the simulation correspond to an "$L$-mode" state.

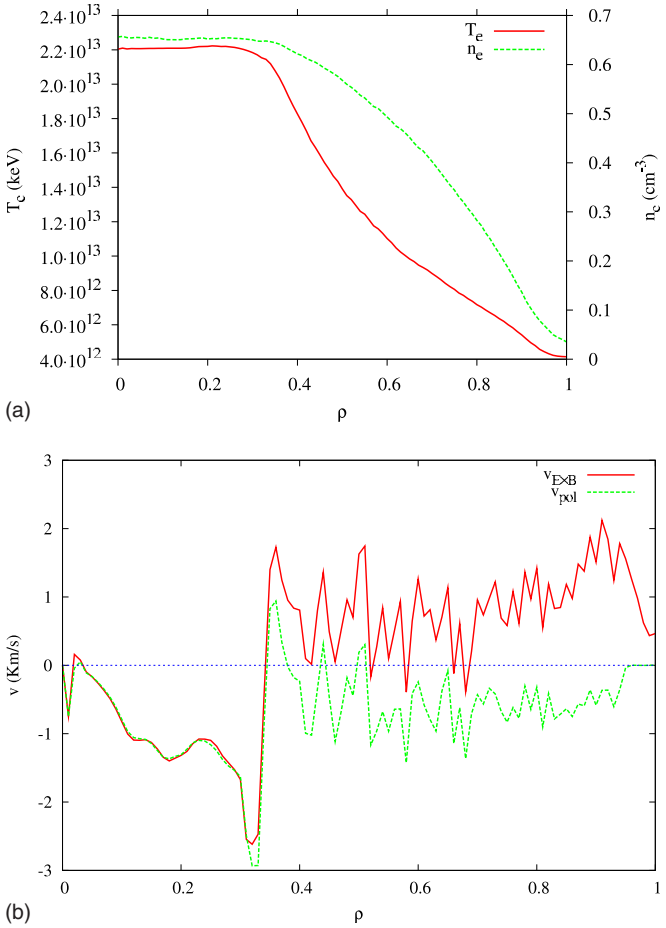


FIG. 1. (Color online) Electron temperature and density (a) and $v_{E\times B}$ and $v_{\mathrm{pol}}$ (b) at $t$=4 ms.

The instantaneous $E\times B$ (poloidal velocity) is plotted in Fig. 1(b) together with the total poloidal velocity, showing a strong shear around $\rho$=0.3, where the slope of the safety factor profile changes and $q \simeq 1$ (see Fig. 2). Note also that the profiles are flat inside $\rho$=0.3. This $q$-profile is not imposed but is an outcome of its coevolution with the turbulence.

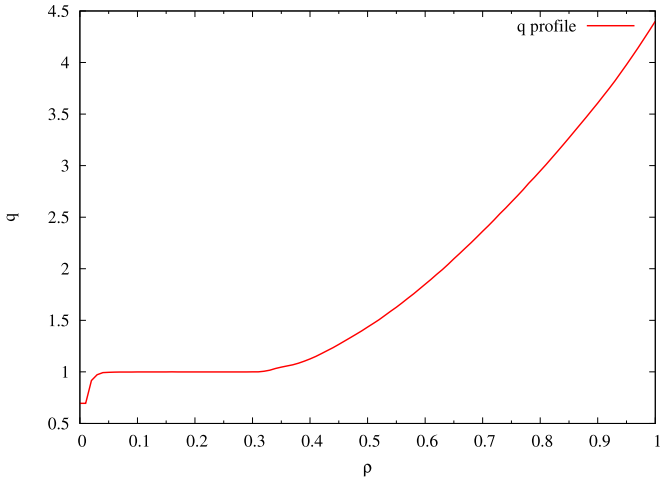


FIG. 2. (Color online) The $q$ profile in CUTIE is approximately constant in time.

Downloaded 11 Aug 2011 to 194.81.223.66. Redistribution subject to AIP license or copyright; see http://pop.aip.org/about/rights_and_permissions

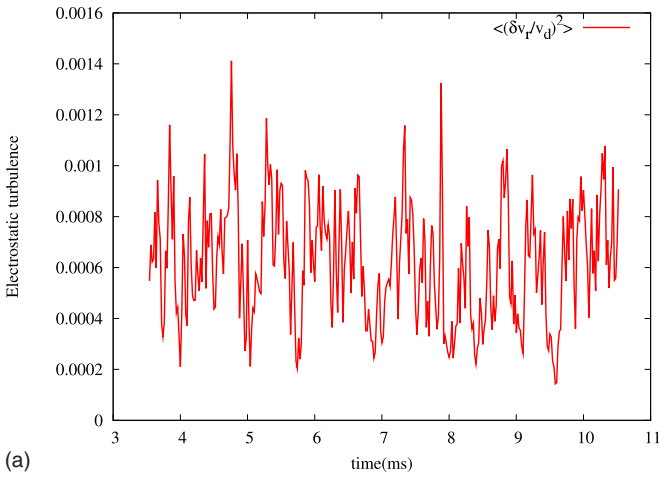


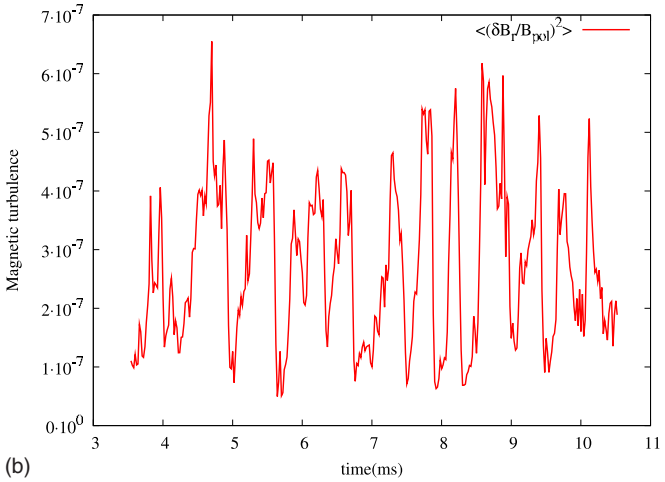


FIG. 3. (Color online) Electrostatic turbulence characterized by $\langle(\delta v_r/v_d)^2\rangle$ (a). Magnetic turbulence characterized by $\langle(\delta B_r/B_{\mathrm{pol}})^2\rangle$ (b).

The electrostatic turbulence level is shown in Fig. 3(a) as the radial velocity fluctuation amplitude normalized by the poloidal drift velocity, while the magnetic turbulence is plotted in Fig. 3(b). The mean turbulence amplitude is not very large. However, there are quasiperiodic events during which the turbulence levels increase sharply. These quasiperiodic events are immediately evident in a figure showing the fluctuation of the electron density (i.e., $\tilde{n}_e = n_e - \langle n_e \rangle$) versus space and time (Fig. 4).

The main quasiperiodic oscillations are generated close to the edge and propagate inward over a long distance. This behavior should of course be reflected in the motion of the tracers we will be studying. We note that Fig. 4 shows that there are at least four regions with separate motion characteristics. The quasiperiodic relaxations propagate from $\rho=0.95$ until $\rho=0.60$ with a barrier located at $\rho=0.80$ ($q=3$). A different behavior is observed inside $q=1$ ($\rho \simeq 0.3$): fluctuations propagate very fast to the axis; however, this region will not be studied here. There is an intermediate region ($0.3<\rho<0.6$) between the surface where the quasiperiodic oscillations stop, and the $q=1$ surface. Here no periodic oscillations are detected.

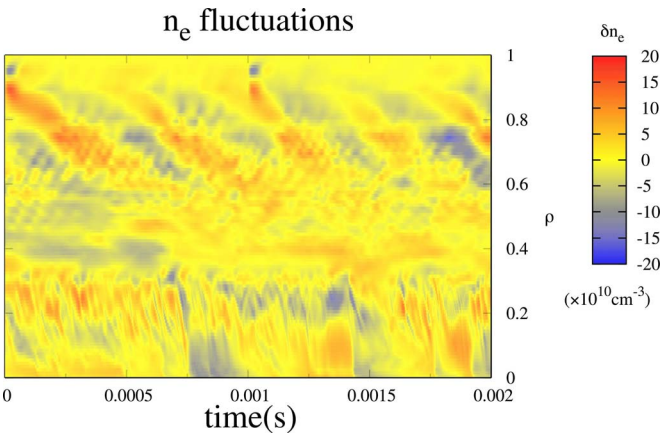


FIG. 4. (Color online) Fluctuations in electron density.

## B. Tracer algorithm

We have injected 10 000 tracers or test particles. In this work, the tracers we use are *ideal*: massless and chargeless. They do not interact with the plasma but are advected passively according to the fluid velocity provided by CUTIE at some grid points. This run was done with a radial mesh of 100 points and using 64 poloidal and 16 toroidal harmonics (the grid being periodic in the poloidal and toroidal directions). Thus, some interpolation is needed to compute the particle trajectories by integration. Three-dimensional spline interpolation has shown to be the most suitable technique because of its computational speed and accuracy. Nevertheless, it was necessary to refine the grid by a factor of 4 in the toroidal direction using Fourier oversampling to improve the spline interpolation results. Integrating these carefully interpolated velocities we then obtain the tracer trajectories, see Fig. 5.

After the turbulence reaches a steady state, all our tracers are launched simultaneously and randomly distributed in the poloidal and toroidal angles on the surface $\rho \equiv r/a = 1/2$. No particles are lost in the time interval simulated.

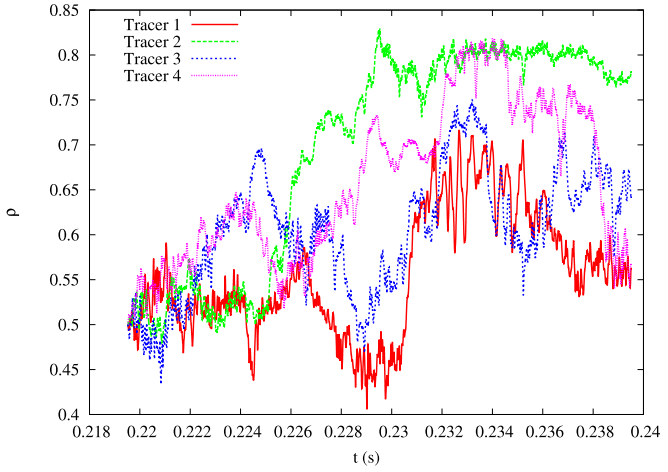


FIG. 5. (Color online) Various radial trajectories.

Downloaded 11 Aug 2011 to 194.81.223.66. Redistribution subject to AIP license or copyright; see http://pop.aip.org/about/rights_and_permissions

### C. Analysis technique I: Distributions

As noted in Sec. I, we will be using the tracers to extract information regarding the particle step and waiting time distributions. Since we expect long-range and long-time correlations to play a significant role, these distributions are expected to be of the Lévy-type,[7,11,32] as we are assuming that these distributions arise from sums of independent and identically distributed variables. This assumption can be verified *a posteriori* from the analysis results. The most important feature of the Lévy distributions is their power-law decay. Thus, we expect

$$p(\Delta\rho) \to C_1|\Delta\rho|^{-(1+\alpha)} \tag{1}$$

for large $\Delta\rho$ values with $C_1$=const and $0<\alpha<2$ ($\alpha=2$ corresponding to a Gaussian distribution[8]) and

$$\psi(\Delta t) \to C_2\Delta t^{-(1+\beta)} \tag{2}$$

with $C_1$=const and $0<\beta<1$ ($\beta=1$ corresponding to an exponential distribution, the Markovian case). The extraction of the parameters $\alpha$ and $\beta$ will be our main goal. The Hurst exponent $H$ is defined as $H\equiv\beta/\alpha$. For $H<\frac{1}{2}$ we say that the motion is subdiffusive; for $H>\frac{1}{2}$ is superdiffusive.[17] Finally, for $H=\frac{1}{2}$ transport is said to be diffusive. However, it is important to stress that ordinary diffusion takes place only when $\alpha=2$ and $\beta=1$. By computing $\alpha$, $\beta$, and $H$ one can say if transport is either standard (diffusive) or nonstandard (fractional) and, in the latter case, these parameters also provide a characterization of the type of long range/long time correlations.

Since we launched the particles at a single radial position and assuming separability of the step and waiting time distributions, their spatial distribution at any given time $p_0(\Delta\rho,t)$ (where $\Delta\rho=\rho-\rho_0$, $\rho_0$ being the center of gravity of the pdf) should reflect the step size distribution $p(\Delta\rho)$ showing the same decay shape and rate, at least, after an initial transient. Thus, we expect $p_0(\Delta\rho,t)\to|\Delta\rho|^{-(1+\alpha)}$ for a range of $\Delta\rho$ values. We have computed $p_0$ using a simple binning procedure by splitting the domain ($0\le\rho\le1$) into bins with a constant size.

Since the binning procedure implies a loss of information (namely, the precise position of each particle), a better method of analysis is provided by the rank function of the radial distribution of the tracers. The rank (or cumulative distribution function) is defined as

$$R(\Delta\rho,t) = \int_{-\infty}^{\Delta\rho} d(\Delta\rho')p_0(\Delta\rho',t). \tag{3}$$

Thus, $R(\Delta\rho,t)$ is the number of particles having $\Delta\rho'<\Delta\rho$ normalized by the total number of particles. It is therefore easily computed by sorting the particles according to their radial position. If the radial distribution decays algebraically as $p_0(\Delta\rho,t)\to|\Delta\rho|^{-(1+\alpha)}$, then the rank function also behaves as a power law: $R(\Delta\rho,t)\to|\Delta\rho|^{-\alpha}$.

Applying a different technique, we have also analyzed tracer motion by artificially decomposing the continuous motion into steps and waiting times. This allows us to compute the step size and waiting time pdfs. This decomposition is done on the basis of a velocity threshold $v_{\text{th}}$, which is arbitrarily introduced. In practice, what we are doing is to reduce radial trajectories to a sequence of flights and trappings, i.e., a CTRW-like trajectory.

The tracer algorithm produces two time series: one for the evolution of the radial position $r(t_i)$ and one for the radial velocity $v_r(t_i)$ of a particle at discrete time intervals $t_i$. We assume that a tracer jumps when its radial velocity is higher than the arbitrary threshold. Between two consecutive jumps there must be at least a zero velocity point (a trapping). We define the radial position of the tracer during the trapping as its mean radial position from the previous jump until the next one. Between two consecutive trappings, no change in the sign of $v_r(t_i)$ is allowed, but on the other hand there may be many points where the absolute tracer velocity exceeds $v_{\text{th}}$. Then, the jump is defined to take place at the time instant with the highest absolute velocity. The jump size is simply the difference of the radial position of the tracer between the preceding and the subsequent trapping.

In summary, this procedure constitutes a method coherent with the intuitive idea of tracers being "trapped" when moving inside an eddy, where the velocity is low and possibly changing sign often, and tracers jumping when their radial velocity is locally maximal. The resulting distributions of waiting times and steps will of course depend on the threshold $v_{\text{th}}$, but within an appropriate range of threshold values the results should be fairly robust, and the threshold value we will be using will be chosen inside this robust range.

In Fig. 6, we show some examples of the reduced trajectories as a function of the threshold. In Fig. 6(a), the threshold velocity is $v_{\text{th}}=100$ m/s. Note that the jumps take place at moments of maximum velocity. The reduced trajectory is a course-grained match to the smooth interpolated trajectory, discarding small oscillations, and with instantaneous jumps in accordance with the philosophy of the CTRW model. As the threshold is increased [see Fig. 6(b)], the number of jumps decreases since a higher radial velocity is needed in order to produce a jump, and the trapping times become longer. Thus, by increasing the threshold we are discarding the smallest displacements for which the tracer can be considered to remain within an eddy; thus, the relative weight of long flights in the distribution $p(\Delta\rho)$ is increased, as well as the weight of long trapping times in $\psi(\Delta t)$.

### D. Analysis technique II: Velocity correlations

Here, we discuss some techniques to measure the self-similarity of the motion by analyzing radial velocities. Figure 7 shows an example of the velocity for a single tracer particle.

Structure functions (SFs) are generalized correlation functions that measure the moments of a distribution. One can apply this analysis technique to study the correlations of the velocity signal $v_r(t_i)$. Following the method suggested in Refs. 33 and 34, the $\nu$-order SF $S_\nu$ of the velocity is defined as

Downloaded 11 Aug 2011 to 194.81.223.66. Redistribution subject to AIP license or copyright; see http://pop.aip.org/about/rights_and_permissions

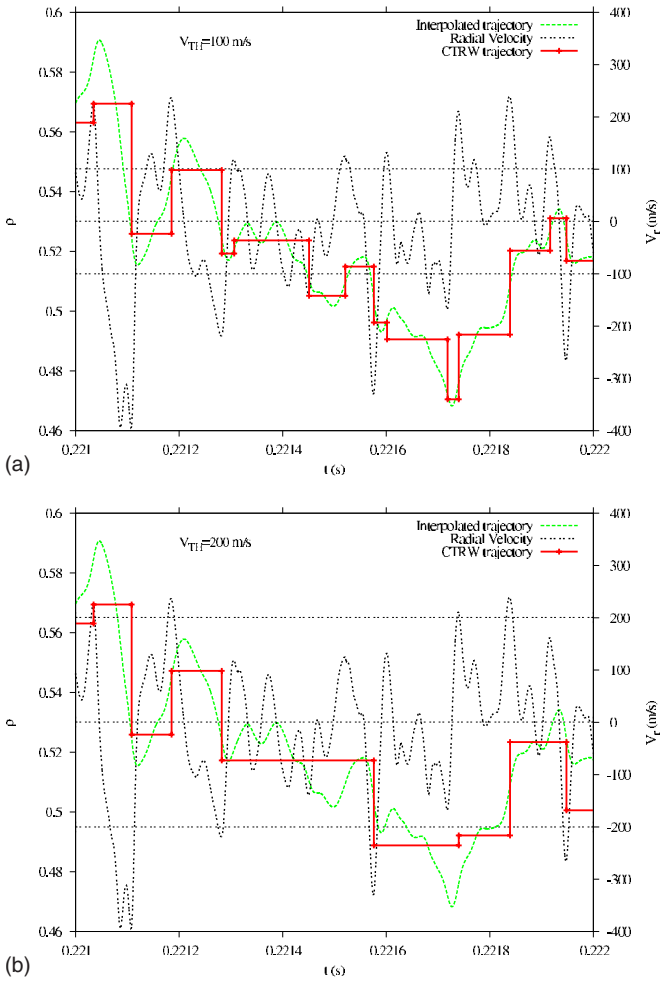


FIG. 6. (Color online) Trajectory as a sequence of jumps and trappings together with velocity for thresholds $v_{th}=100$ m/s (a) and $v_{th}=200$ m/s (b).

$$S_\nu(\tau) \equiv \langle |v_r(t_i+\tau) - v_r(t_i)|^\nu \rangle \tag{4}$$

for any time interval $\tau$, where $\langle\cdot\rangle$ is the average value. Assuming that the $v_r$ time series is scale invariant and monofractal, there should be an interval of $\tau$ values $\tau_1 < \tau < \tau_2$, where $S_\nu$ should satisfy

$$S_\nu(\tau) \propto \tau^{\nu \cdot H}. \tag{5}$$

Deviations from this property may indicate nonstationarity or multifractality.

The Lagrangian velocity correlation function also provides information on $H$. However, instead of calculating it directly, we use a technique that is more suitable to scarce data, namely, the rescaled range (R/S) technique, following the method detailed in Ref. 35.

We determine the $R/S$ curve for every single particle along its trajectory. $R$ is the maximal range of the integrated particle velocity with respect to a reference and $S$ is an $s$-order moment of the velocity. $s$ is taken such that $s<\alpha$ (previously calculated), so $R/S$ measures the maximum deviation respect to the mean dispersion. Given an interval of $n$ consecutive instant velocities of the tracer $[v_r(t_1), v_r(t_2), \ldots, v_r(t_n)]$, the definition is

$$\frac{R(n)}{S(n)} = \frac{\max(0, W_1, W_2, \ldots, W_n) - \min(0, W_1, W_2, \ldots, W_n)}{\langle |V_r(n)|^s \rangle^{1/s}}, \tag{6}$$

where $W_k$ is

$$W_k = \sum_{i=1}^{k} v_r(t_i) - k\langle v(n) \rangle. \tag{7}$$

We calculate $R(n)/S(n)$ for different $n$ values ($n$ corresponding to a time interval of length $\tau_n = n\Delta t$, where $\Delta t$ is the time step of the time series) for every single tracer trajectory. Averaging over many tracers one expects the following scaling relation to hold (over a relevant scaling range):

$$\left\langle \frac{R(n)}{S(n)} \right\rangle_{n\to\infty} \to \tau_n^H. \tag{8}$$

Another approach to the analysis of velocity correlations is the study of the "cumulative velocity" or distribution $p(d)$ of the total displacement $d$ in a fixed time $\tau_M$, as in Ref. 17. Indeed, as we will show, we detect long range correlations for large values of $\tau_M < \tau_{tot}$; at large values of $\tau_M$ the influence of the cutoff due to the finite length of the simulation distorts the distribution. This technique allows the measurement of $\alpha$ since one expects the distribution to scale like $p(d) \to C_3 d^{-(1+\alpha)}$ for large $d$.

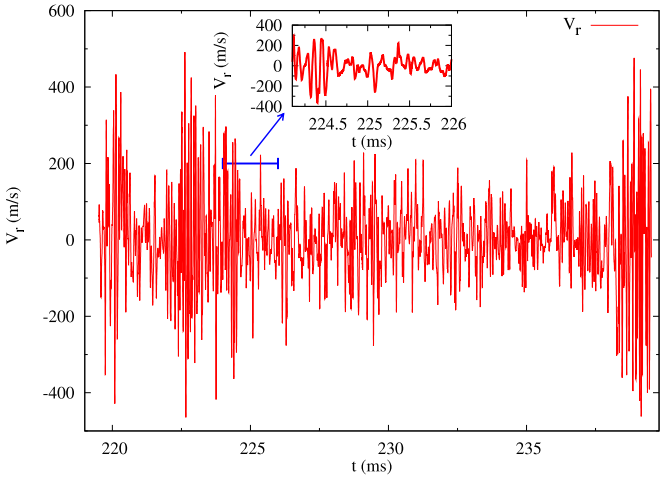


FIG. 7. (Color online) Velocity of a particle during the whole simulation and a 2 ms detail.

## III. RESULTS

### A. Probability distribution function

In Fig. 8 we show the pdf at different times. Note the existence of a transport barrier: tracers seem to be unable to cross $\rho \approx 0.8$ and tend to accumulate just below this radial point. In addition, there is a global outward drift of the distribution (a gradual shift in the peak value). These facts, together with the fact that the curve is quite rough, make the detection of any power law decay difficult. However, toward the inside, a tail with slow decay is observed, which looks non-Gaussian. When attempting to fit this tail to a power-law

Downloaded 11 Aug 2011 to 194.81.223.66. Redistribution subject to AIP license or copyright; see http://pop.aip.org/about/rights_and_permissions

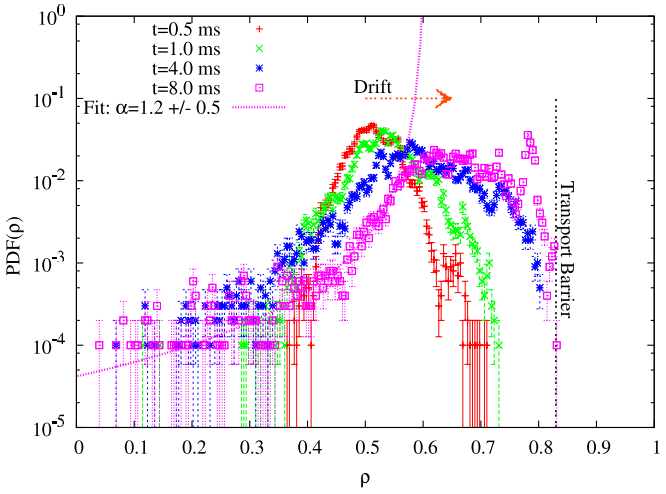


FIG. 8. (Color online) Radial distribution of tracers and fit of the left tail at $t=8.0$ ms.

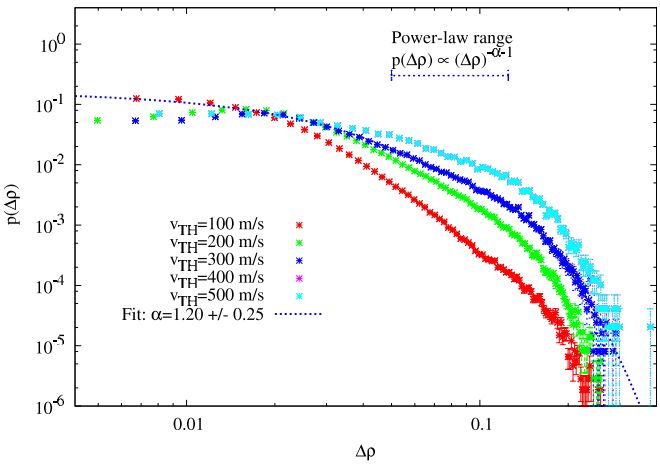


FIG. 10. (Color online) Step size pdf for different $v_{th}$ in log-log scale and step size normalized to minor radius. Best power-law fit for $v_{th}=300$ m/s.

function $p(\Delta\rho)=A\cdot|\Delta\rho|^{-(1+\alpha)}$, we find that the fit is not very robust, and consequently the parameter $\alpha$ can only be determined with a large associated error: $\alpha=1.2\pm0.5$.

The following analysis is strongly weighted toward the $\rho$ range where the population of tracers is statistically significative, i.e., $0.3<\rho<0.8$.

## B. Rank

In Fig. 9 we show the rank function corresponding to the pdf at $t=8$ ms plotted in Fig. 8. The rank function can be fitted to a power law in an appropriate $\Delta\rho$ interval as Fig. 9 shows. The fit is rather good and yields $\alpha=1.43\pm0.11$. At later times than the time shown, the distribution becomes strongly distorted due to the influence of the transport barriers associated with the $q$-profile and finite-size effects so that no useful fit is possible. The results therefore pertain to what might be called an "intermediate" state of dispersion of the particles, namely, after the initial transient effects have died out and before distortion due to finite-size effects sets in.

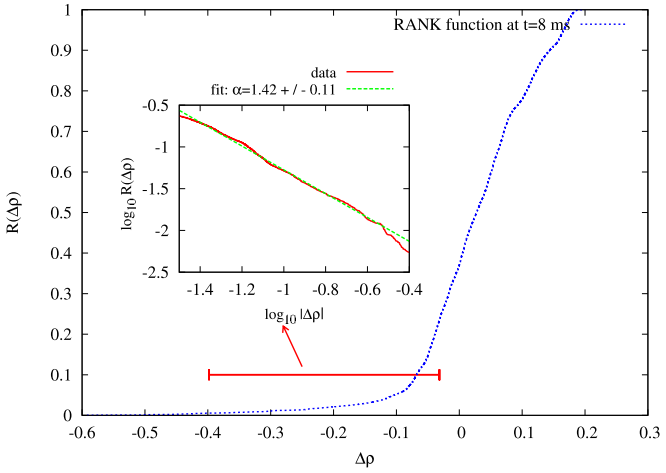


FIG. 9. (Color online) Rank function and power law fit interval. Inset: data from fit interval and fit.

## C. Step size pdf

We have stored, classified, and analyzed the jumps and waiting times of all tracers for 20 ms simulation with the algorithm detailed in Sec. II C. First, we computed the step size distribution for different thresholds, see Fig. 10.

For low threshold velocities, the local eddy motion dominates the transport so that the distributions decay relatively fast ($v_{th}\leq200$ m/s). A moderately high $v_{th}$ is needed to filter out short-range motion and obtain Lévy-type pdfs decaying as $p\rightarrow\Delta\rho^{-(1+\alpha)}$. Nevertheless, the relatively low number of radial grid points in CUTIE restricts the power-law range that can be obtained. This finite-size effect becomes dominant for high $v_{th}$ (irregular shape, shorter power-law range in Fig. 10 for $v_{th}\geq400$ m/s). However, for an intermediate velocity threshold, $v_{th}=300$ m/s, a relatively clear power law is observed. For low $v_{th}$, we note that as the threshold increases $\alpha$ gets smaller. It seems to stabilize for $v_{th}\geq300$ m/s.

To fit the whole curve, we define a fit function consisting of three sections (exponential—power law—exponential), where the power-law interval (between $\Delta\rho_1$ and $\Delta\rho_2$) is variable. The fit function is restricted to be continuous at the matching points $\Delta\rho_1$ and $\Delta\rho_2$. This method is free from bias when selecting the power-law fit range and turned out to provide stable results. Thus, we obtained $\alpha=1.20\pm0.25$.

## D. Waiting time pdf

When computing the waiting time distribution function, we note that there is an important difference with respect to the step size distribution: while local eddy motion again dominates the process for low $v_{th}$, the finite size effect for high velocity thresholds is much less restrictive, since the only limit on the waiting times is the total length of the simulation (see Fig. 11).

Thus, the waiting time distributions show a very long algebraic tail (longer than a decade), so the $\beta$ parameter can be determined with good accuracy by fitting the pdfs to a function $\psi(\Delta t)\propto\Delta t^{-(1+\beta)}$. The best fit (larger power-law range, smaller relative associated error) is obtained for $v_{th}$

Downloaded 11 Aug 2011 to 194.81.223.66. Redistribution subject to AIP license or copyright; see http://pop.aip.org/about/rights_and_permissions

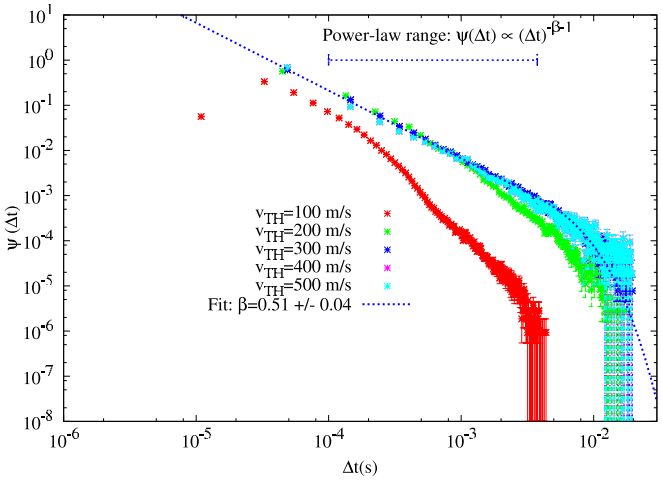


FIG. 11. (Color online) The waiting time pdf for different $v_{th}$ in log-log scale. The total simulation time is 20 ms. Best power-law fit for $v_{th}=300$ m/s.

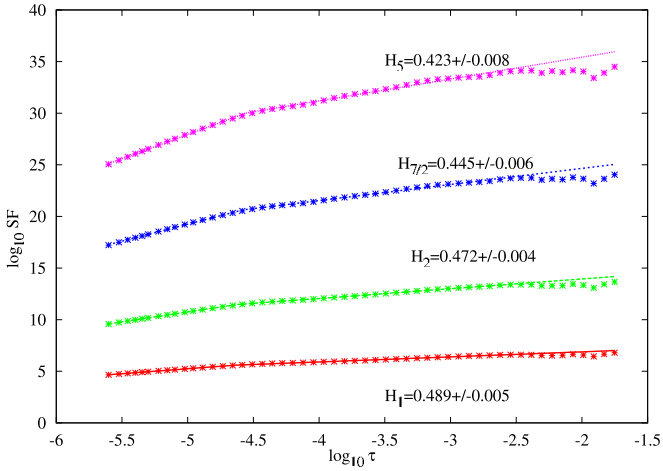


FIG. 13. (Color online) Example of the SF ($SF_\nu$) for the velocity of a tracer in log-log scale for several orders $\nu$ and fits.

$=300$ m/s (identical to the value selected for the best step size pdf fit). Now, the data are fitted to a continuous function consisting of two regions: power law/exponential. We obtain $\beta=0.51\pm0.05$. $\beta$ and $\alpha$ show a similar dependence on $v_{th}$.

The pdf corresponding to the lowest value of $v_{th}$ shown can be fitted for small $\Delta t$ to an exponential distribution $\psi(\Delta t)\propto\exp(-\Delta t/\tau_{ED})$ (Fig. 12). The value of the fit parameter is $\tau_{ED}=(9.6\pm0.3)\times10^{-5}$ s, which we interpret as the eddy turnover time. $\tau_{ED}$ corresponds well with the turbulence decorrelation time $t_d$. In this CUTIE run, $t_d\sim30-90$ $\mu$s from the analysis of the autocorrelation of electron density.

### E. Structure functions

We computed the SFs of order $\nu=1/2,1,3/2,\ldots,5$ for the velocity for every single tracer over the whole simulation time ($\tau_{tot}$). In Fig. 13 an example is shown.

The SFs are fitted by a function consisting of two connected power-law sections, discarding time lags $\tau>2.5$ ms. In the first section ($\tau<\tau_{1(SF)}$), $H\approx1$, but for $\tau\geq\tau_{1(SF)}$ we get approximately diffusive values for $H$. Interestingly, the connection point between the two regions is $\tau_{1(SF)}\sim\tau_{ED}$, as it should be. Lag times larger than $t_d$ are needed to measure the self-similarity of the motion. $H$ is fairly constant with $\nu$ with perhaps a slight tendency to decay with increasing $\nu$. We averaged over all tracers and orders to obtain a mean estimate of $H$ and obtained $H=0.452\pm0.019$.

### F. Lagrangian correlation

We have calculated $H$ using the R/S method, as explained in Sec. II D. We averaged over all tracer trajectories to minimize the error in the result. As it seems that $\alpha>1$, we take $s=1$. Figure 14 shows an example.

In this case, the best fit result is obtained by using a fit function consisting of three connected power-law sections. For lag times shorter than $\tau_{1(RS)}\approx100$ $\mu$s we obtain $H\approx1$. For lag times comparable to $\tau_{tot}$, we obtain $H\approx0$, while in the intermediate region we detect approximately diffusive behavior. When averaging the individual $H$ values of all tracers in the intermediate region, we obtain $\langle H\rangle=0.54\pm0.05$.

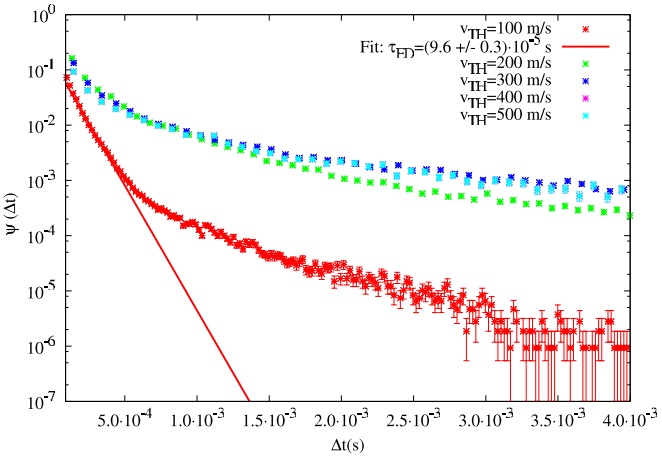


FIG. 12. (Color online) The waiting time pdf for different $v_{th}$ in log-lin scale. For low $v_{th}$, transport is dominated by local eddy motion.

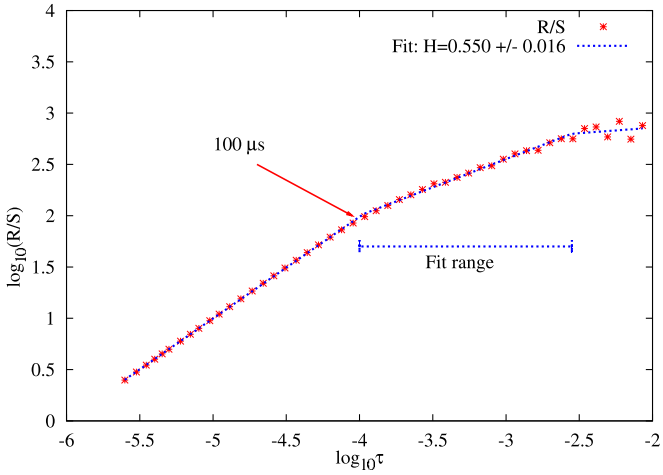


FIG. 14. (Color online) Example of the R/S technique applied to the velocity of a tracer in log-log scale and fit.

Downloaded 11 Aug 2011 to 194.81.223.66. Redistribution subject to AIP license or copyright; see http://pop.aip.org/about/rights_and_permissions

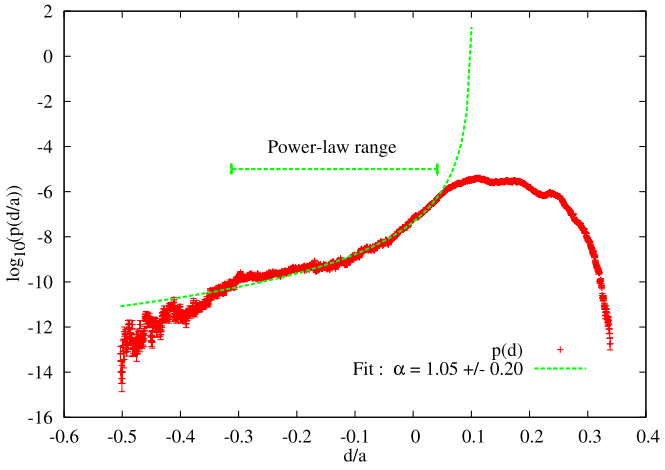


FIG. 15. (Color online) Distribution of total radial displacements in $\tau_M = 5$ ms and fit.

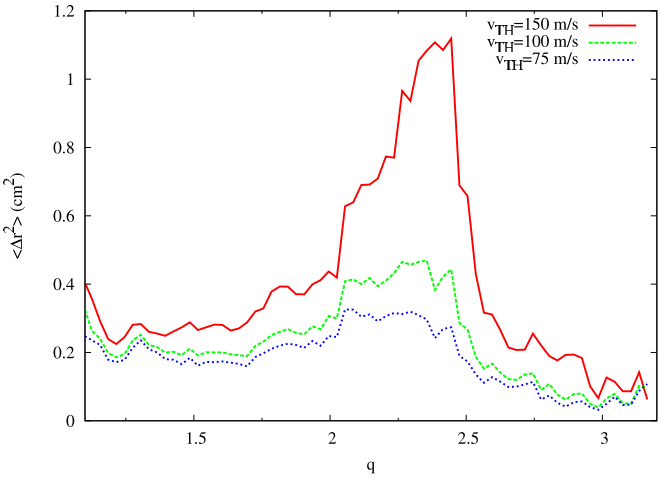


FIG. 17. (Color online) $\langle \Delta r^2 \rangle(q)$ for different $v_{\text{th}}$.

The (connection) points where the slopes change with both the R/S and the SF techniques are quite similar. This time also coincides with the eddy turnover time measured in the waiting time pdf analysis and with the turbulence decorrelation time: $t_d \sim 30-90$ $\mu$s.

By analyzing the cumulative velocity distribution we obtain another measure of $\alpha$. This analysis is similar to the analysis of the pdf and rank functions presented above but independent of the choice of the tracer injection point $\rho_0$. The best fit is obtained for $\tau_M = 5$ ms, see Fig. 15. Again, because of the global outward drift, the transport barrier near $\rho = 0.8$, and the finite size effect, only the inward tail of the pdf is useful, and the best fit corresponds to $\alpha = 1.05 \pm 0.20$. Figure 15 suggests that the longest excursions of the tracers are mainly inward. This is in good qualitative agreement with the global propagation observed in Fig. 4. Furthermore, the similarity between this figure and Fig. 8 indicates a close match between individual and collective motion.

### G. The *q*-profile

We already noted in several places that the $q$-profile (Fig. 2) appears to influence the transport of the tracers. The first indication of this effect is obtained when computing the radial distribution of the tracers. After a few milliseconds of simulation, the shape of the pdf changes dramatically close to some rational surfaces, see Fig. 16.

To bring this out more clearly, we have plotted $p_0(q)$ instead of $p_0(\rho)$ by applying a simple change in variables. Only the range $q > 1$ is taken into account, since $q$ is essentially flat in the innermost region and because of the poor statistics at $q \leq 1$. We note that the distribution changes sharply around $q = 3/2, 2, 5/2, 3$, and possibly some other values of $q$. In addition, there is a sharp decay at $q = 11/4$.

In an attempt to quantify the effect of $q$ on transport, we have computed the mean square step length $\langle \Delta r^2 \rangle$ as a function of $q$ at the point where the particle jumps, see Fig. 17. To do so, we used the algorithm described in Sec. II C (see Fig. 6) for different threshold velocities.

Evidently, the graph of $\langle \Delta r^2 \rangle(q)$ is nontrivial. There are

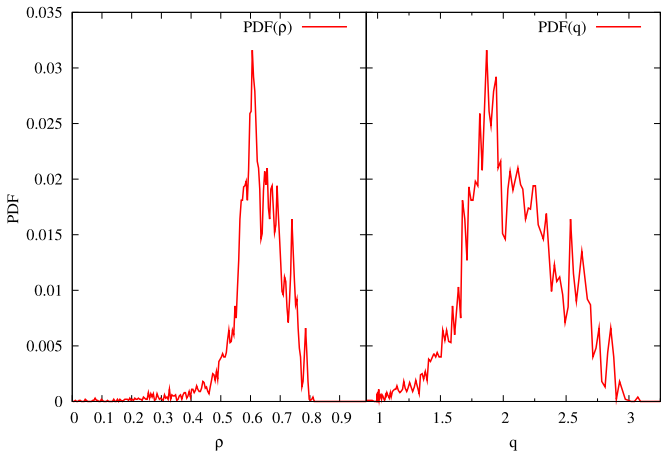


FIG. 16. (Color online) $p_0(\rho)$ and $p_0(q)$ after 5 ms.

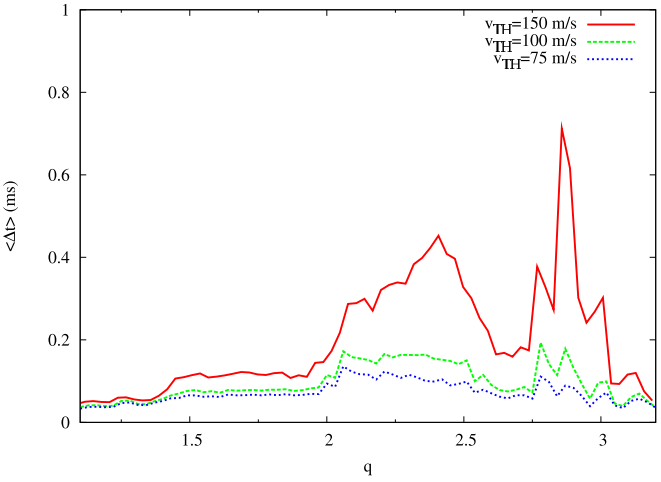


FIG. 18. (Color online) $\langle \Delta t \rangle(q)$ for different $v_{\text{th}}$.

Downloaded 11 Aug 2011 to 194.81.223.66. Redistribution subject to AIP license or copyright; see http://pop.aip.org/about/rights_and_permissions

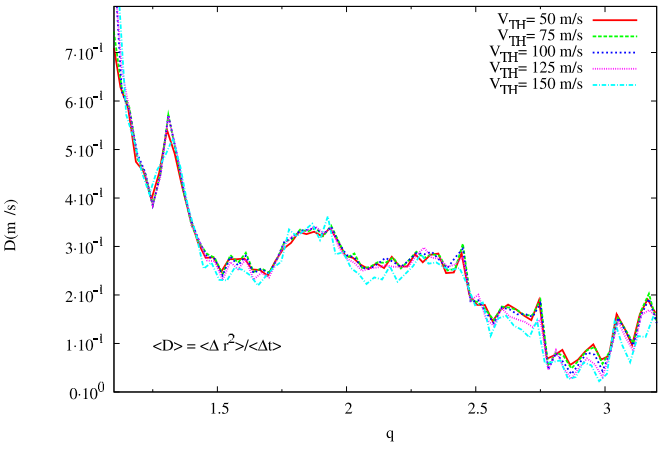


FIG. 19. (Color online) Standard diffusion: mixing length diffusion coefficient for different $v_{th}$.

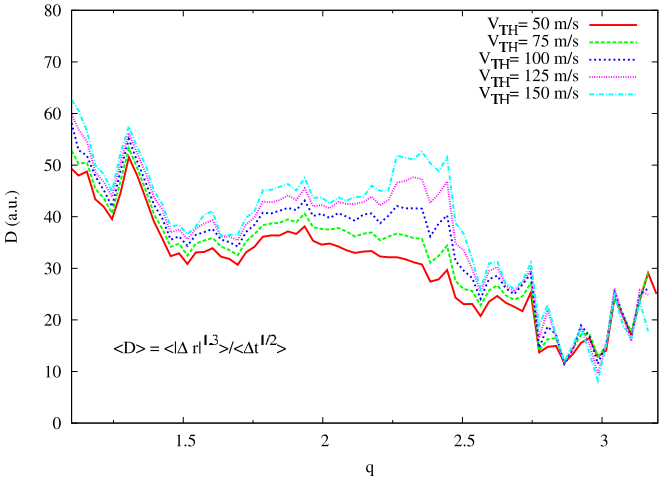


FIG. 20. (Color online) Fractional diffusion: effective diffusion coefficient for different $v_{th}$.

strong slope variations around the rational surfaces $q=2,5/2,3$, and possibly others. These changes are enhanced as the threshold is raised.

A similar analysis can be made for the waiting time distribution. We computed the dependence of the mean waiting times of the tracers on $q$, i.e., $\langle \Delta t \rangle(q)$, see Fig. 18. The slope of this magnitude changes drastically at $q=3/2$, 2, 5/2, 11/4, and 3 similar to $p(q)$: with increasing $q$, $\langle \Delta t \rangle$ is approximately constant until $q=3/2$, where it increases. Then, it is constant until about $q=2$, where $\langle \Delta t \rangle$ increases again. It then grows slowly until it drops around $q=5/2$ then rises sharply near $q=11/4$ and finally falls back at $q=3$. These variations are complex and not fully understood, although the relationship with $q$ is beyond question. Again, the variations are enhanced by raising the velocity threshold, suggesting that these effects are more important for the longer waiting times. We also note that the radial evolution of $\langle \Delta r^2 \rangle(q)$ is slightly different from the radial evolution of $\langle \Delta t \rangle(q)$, suggesting different mechanisms are involved (at least in part).

Using the preceding results, it is not difficult to deduce an effective diffusion coefficient. Assuming that transport is diffusive $(\alpha=2,\beta=1)$, the diffusion coefficient can be estimated using the mixing length argument[36]

$$D = \sigma^2/\tau_D, \tag{9}$$

where $\sigma$ is the characteristic step size and $\tau_D$ is the characteristic waiting time. Taking $\sigma^2=\langle \Delta r^2 \rangle$ and $\tau_D=\langle \Delta t \rangle$, the resulting diffusion coefficient is shown in Fig. 19.

Remarkably, the mixing length diffusion coefficient shows no dependence on $v_{th}$ and is, on average, decreasing as one moves to the edge. This decreasing trend is obviously related to the presence of transport barriers at high values of $q$ and to the inward propagating (ballistic) events mentioned earlier. The slope variations observed in the previous plots persist and occur at the same rational surfaces as before.

On the other hand, in the context of the fractional diffusive equation with values $\alpha$ and $\beta$ different from the standard diffusive values, an effective (fractional) diffusion coefficient can be estimated following Ref. 37,

$$D_{\alpha,\beta} = \sigma^\alpha/\tau_D^\beta, \tag{10}$$

where $\sigma^2=\langle \Delta r^\alpha \rangle$ and $\tau_D=\langle \Delta t^\beta \rangle$. We have also calculated this alternative diffusion coefficient considering the values of $\alpha$ and $\beta$ that we obtained from our previous analysis. So, in Fig. 20 the diffusion coefficient is plotted for $\alpha=1.3$ and $\beta=0.5$. Now, we observe a mild dependence of the results on $v_{th}$. In Fig. 20, the effect of the rational surfaces on transport becomes more evident for increasing $v_{th}$. Note that Figs. 19 and 20 have a fairly similar overall shape.

As has been observed experimentally,[38–40] we find that transport is sensitive to the presence of rational surfaces. This has been observed before in CUTIE simulations[24,25,27] but never using tracer particles.

## H. Summary

In the course of this paper, several tracer analysis techniques have been applied in order to determine the effective nature of the transport in a particular CUTIE run with turbulence. All our methods were applied to the same set of particle trajectories. As a consequence, it appears that the effective transport does not fulfill the standard assumption that transport is local and Markovian. In Table I we have collected the various results for ease of comparison. Combining the results obtained with the various techniques, we find (last row of the table) $\alpha \simeq 1.32$, $\beta \simeq 0.51$, and $H \simeq 0.46$.

TABLE I. Compilation of results.

| Technique | $\alpha$ | $\beta$ | $H$ |
|---|---|---|---|
| pdf analysis | $1.2 \pm 0.5$ | | |
| Rank function | $1.43 \pm 0.11$ | | |
| Jump size distribution | $1.20 \pm 0.25$ | | |
| Waiting time distribution | | $0.51 \pm 0.04$ | |
| SFs | | | $0.452 \pm 0.019$ |
| Lagrangian analysis | $1.05 \pm 0.20$ | | $0.54 \pm 0.05$ |
| Best estimate | $1.32 \pm 0.09$ | $0.51 \pm 0.04$ | $0.46 \pm 0.02$ |

Downloaded 11 Aug 2011 to 194.81.223.66. Redistribution subject to AIP license or copyright; see http://pop.aip.org/about/rights_and_permissions

To check the consistency of these results, we calculate $H$ using the relationship $H=\beta/\alpha$. Taking the best estimates of $\alpha$ and $\beta$ from Table I, we get $H=0.39\pm0.04$, consistent with the best value of $H$ listed in the table.

Since $\alpha\simeq1.32<2$ the effective transport is nonlocal, which is doubtlessly related to the effect of the "avalanche-like" inward propagating quasiperiodic events shown in the plot of $\tilde{n}_e$. Likewise, since $\beta\simeq0.51<1$, the effective transport is non-Markovian, which is probably related to the existence of transport barriers (trapping regions) associated with the rational $q$-surfaces (cf. Ref. 41), as we have shown. Indeed, when attempting to calculate effective transport parameters, it is evident that the transport level is strongly affected when crossing particular rational surfaces.

## IV. DISCUSSION AND CONCLUSIONS

Applying a wide range of analysis techniques to the motion of tracers in a CUTIE simulation of plasma turbulence, we find that the effective global transport is clearly nonlocal and non-Markovian.

We note that our results are similar to the results obtained by other authors in equivalent studies, most of them in pressure-gradient-driven plasma turbulence. In Ref. 2, the authors deal with a resistive ballooning mode driven by pressure gradients in toroidal geometry, and obtain $\alpha\approx1.1$ by studying the pdf and $H\approx0.6$ with Lagrangian analysis, i.e., $\beta\approx0.7$. Our value of $\alpha$ is rather similar but we find a much lower $\beta$ and $H$. Likewise, the authors in Ref. 3 obtained $\alpha\approx0.75$, $\beta\approx0.5$, and thus $H\approx0.66$. Here, the underlying instability is the resistive interchange mode driven by pressure gradients in cylindrical geometry. In this case, $\alpha$ and $H$ are different than what we found in CUTIE, while $\beta$ matches up very well with our results displayed in Table I. In another tracer study of a pressure gradient driven turbulence model, a much higher value for $H$ was obtained: in Ref. 1, the authors obtained $H\approx0.88$ (superdiffusion) and $\beta\approx0.81$ from the waiting time distribution, i.e., $\alpha\approx0.92$. We note that this set of parameters is rather different from our results. In a study of dissipative-trapped-electron-mode turbulence,[4] different sets of $\alpha$, $\beta$, and $H$ values are obtained. However, a diffusive value for $H$ is only obtained with $\alpha\lesssim2$ and $\beta\approx0.5$.

In summary, some of our particular values are relatively similar to other authors' ($\alpha$ in Ref. 2 or $\beta$ in Ref. 3). However, globally our measurements do not match with most of the other published results, where transport is superdiffusive instead of approximately diffusive (in terms of $H$, not $\alpha$, $\beta$) or mildly subdiffusive as we find in CUTIE. We note that our results may also be influenced slightly by the existence of different radial transport zones, although they are heavily weighted toward the midradius zone ($0.4<\rho<0.8$), since that is where the majority of particles analyzed reside.

However, since various and different types of turbulence are considered in the mentioned studies, perhaps it is not to be expected that similar results should be obtained. In this respect, note that our work presents an important difference with respect to the cited studies: CUTIE models a plasma considering several turbulent modes simultaneously while other works deal with only one. In this sense, our simulation is "more realistic" since in actual plasmas several turbulent modes are expected to be active. Further studies (e.g., involving the deactivation of some instabilities) may clarify whether the presence of this wide range of instabilities has any particular effect on the results we obtain.

Another path we propose to explore in the near future is the modeling of nonideal tracers (i.e., impurities having mass and charge) in order to prepare for actual impurity injection experiments for transport studies in the vein of the present work.

Finally, the observed correlation between the safety factor and the radial transport of tracers not only indicates what influence low order rational surfaces may have on particle motion, but is also reminiscent of the phenomenological *q-comb* model[39] that has been invoked to explain some heat transport phenomena.

## ACKNOWLEDGMENTS

The authors would like to thank the TJ-II team for their support and R. Sánchez, I. Calvo, J. A. Mier, D. E. Newman, and V. Tribaldos for stimulating discussions. This research was sponsored in part by Dirección General de Investigaciones Científicas y Tecnológicas (DGICYT) of Spain under Project No. ENE2006-15244. Research of A.T. was funded jointly by United Kingdom Engineering and Physical Sciences Research Council and the contract of association between EURATOM and UKAEA. The views and opinions expressed herein do not necessarily reflect those of the European Commission.

[1] B. Carreras, V. Lynch, and G. Zaslavsky, Phys. Plasmas **8**, 5096 (2001).
[2] L. García and B. Carreras, Phys. Plasmas **13**, 022310 (2006).
[3] D. del Castillo-Negrete, B. Carreras, and V. Lynch, Phys. Plasmas **11**, 3854 (2004).
[4] J. Mier, R. Sánchez, L. García, D. Newman, and B. Carreras, Phys. Plasmas **15**, 112301 (2008).
[5] E. Montroll and G. Weiss, J. Math. Phys. **6**, 167 (1965).
[6] W. Shugard and H. J. Reiss, J. Chem. Phys. **65**, 2827 (1976).
[7] R. Balescu, Phys. Rev. E **51**, 4807 (1995).
[8] R. Sánchez, B. van Milligen, D. Newman, and B. Carreras, Phys. Rev. Lett. **90**, 185005 (2003).
[9] B. van Milligen, R. Sánchez, and B. Carreras, Phys. Plasmas **11**, 2272 (2004).
[10] B. van Milligen, B. Carreras, and R. Sánchez, Phys. Plasmas **11**, 3787 (2004).
[11] R. Balescu, *Aspects of Anomalous Transport in Plasmas* (Institute of Physics, University of Reading, Berkshire, 2005), p. 423.
[12] V. Kenkre, E. Montroll, and M. Shlesinger, J. Stat. Phys. **9**, 45 (1973).
[13] J. Klafter and R. Silbey, Phys. Rev. Lett. **44**, 55 (1980).
[14] R. Metzler and J. Klafter, Phys. Rep. **339**, 1 (2000).
[15] G. Zaslavsky, Phys. Rep. **371**, 461 (2002).
[16] R. Sánchez, B. van Milligen, and B. Carreras, Phys. Plasmas **12**, 056105 (2005).
[17] R. Sánchez, B. Carreras, D. Newman, V. Lynch, and B. van Milligen, Phys. Rev. E **74**, 016305 (2006).
[18] I. Calvo, B. Carreras, R. Sánchez, and B. van Milligen, J. Phys. A: Math. Theor. **40**, 13511 (2007).
[19] I. Calvo, R. Sánchez, B. Carreras, and B. van Milligen, Phys. Rev. Lett. **99**, 230603 (2007).
[20] I. Calvo, L. García, B. Carreras, R. Sánchez, and B. van Milligen, Phys. Plasmas **15**, 042302 (2008).
[21] B. van Milligen, I. Calvo, and R. Sánchez, J. Phys. A: Math. Theor. **41**, 215004 (2008).
[22] A. Thyagaraja, P. Knight, M. de Baar, G. Hogeweij, and E. Min, Phys. Plasmas **12**, 090907 (2005).
[23] P. Mantica, A. Thyagaraja, J. Weiland, G. Hogeweij, and P. Knight, Phys.

Downloaded 11 Aug 2011 to 194.81.223.66. Redistribution subject to AIP license or copyright; see http://pop.aip.org/about/rights_and_permissions

Rev. Lett. **95**, 185002 (2005).
[24]L. Garzotti, X. Garbet, A. Thyagaraja, M. de Baar, D. Frigione, P. Mantica, V. Parail, B. Pégourié, L. Zabeo, and JET EFDA Contributors, Nucl. Fusion **46**, 73 (2006).
[25]A. Thyagaraja, P. Knight, and N. Loureiro, Eur. J. Mech. B/Fluids **23**, 475 (2004).
[26]G. Hogeweij, A. Oomens, C. Barth, M. Beurskens, C. Chu, J. van Gelder, J. Lok, N. Lopes Cardozo, F. Pijper, R. Polman, and J. Rommers, Phys. Rev. Lett. **76**, 632 (1996).
[27]M. de Baar, A. Thyagaraja, G. Hogeweij, P. Knight, and E. Min, Phys. Rev. Lett. **94**, 035002 (2005).
[28]R. E. Waltz, J. Candy, and C. C. Petty, Phys. Plasmas **13**, 072304 (2006).
[29]S. Fielding, P. Carolan, J. Connor, N. Conway, A. Field, P. Helander, Y. Igitkhanov, B. Lloyd, H. Meyer, A. Morris, O. Pogutse, M. Valovi, H. Wilson, COMPASS-D Team, and ECRH Team, Nucl. Fusion **41**, 909 (2001).
[30]M. Valovic, P. Carolan, A. Field, S. Fielding, P. Jones, B. Lloyd, H. Meyer, M. Price, V. Shevchenko, K. Stammers, M. Walsh, S. You, COMPASS-D Team, and ECRH Team, Plasma Phys. Controlled Fusion **44**, A175 (2002).
[31]A. Colton, R. Buttery, S. Fielding, T. Hender, P. Leahy, and A. Morris, Nucl. Fusion **39**, 551 (1999).
[32]B. Gnedenko and A. Kolmogorov, *Limit Distributions for Sums of Independent Random Variables* (Addison-Wesley, Reading, MA, 1954), p. 162.
[33]M. Gilmore, C. Yu, T. Rhodes, and W. Peebles, Phys. Plasmas **9**, 1312 (2002).
[34]C. Yu, M. Gilmore, W. Peebles, and T. Rhodes, Phys. Plasmas **10**, 2772 (2003).
[35]B. Carreras, B. van Milligen, M. Pedrosa, R. Balbín, C. Hidalgo, D. Newman, E. Sánchez, M. Frances, I. García-Cortés, J. Bleuel, M. Endler, S. Davies, and G. Matthews, Phys. Rev. Lett. **80**, 4438 (1998).
[36]B. van Milligen, B. Carreras, and R. Sánchez, Plasma Phys. Controlled Fusion **47**, B743 (2005).
[37]R. Sánchez, B. Carreras, and B. van Milligen, Phys. Rev. E **71**, 011111 (2005).
[38]B. Pegourie and M. Dubois, Nucl. Fusion **29**, 745 (1989).
[39]N. Lopes Cardozo, G. Hogeweij, M. de Baar, C. Barth, M. Beurskens, F. De Luca, A. Donné, P. Galli, J. van Gelder, G. Gorini, B. de Groot, A. Jacchia, F. Karelse, J. de Kloe, O. Kruijt, J. Lok, P. Mantica, H. van der Meiden, A. Oomens, T. Oyevaar, F. Pijper, R. Polman, F. Salzedas, F. Schüller, and E. Westerhof, Plasma Phys. Controlled Fusion **39**, B303 (1997).
[40]E. Joffrin, C. Challis, T. Hender, D. Howell, and G. Huysmans, Nucl. Fusion **42**, 235 (2002).
[41]J. Misguich, J.-D. Reuss, D. Constantinescu, G. Steinbrecher, M. Vlad, F. Spineanu, B. Weyssow, and R. Balescu, Ann. Phys. Fr. **28**, 1 (2003).

**Downloaded 11 Aug 2011 to 194.81.223.66. Redistribution subject to AIP license or copyright; see http://pop.aip.org/about/rights_and_permissions**